Heat Generation in the Inertia Welding of Dissimilar Tubes

A reduced thermal model is developed that accurately captures joint temperatures and provides guidance in weld parameter development

BY V. R. DAVÉ, M. J. COLA, AND G. N. A. HUSSEN

ABSTRACT. The transient thermal response in inertia welding is difficult to capture analytically. Heat is generally dissipated over time scales of less than one second, an order of magnitude faster than direct-drive friction welding. The present work critically examines the nature of the heat generation term through an analysis of experimental data. The method presented here determines the heat generation term for the inertia welding of dissimilar tubes (tube thickness small in comparison to radius so that radial effects are neglected) solely based on machine-generated data, namely the curve of angular speed vs. time and the magnitude of material burnoff. A simple approach to determining the heat allocation to both sides of the dissimilar joint is proposed, and the resulting thermal problem is solved using an analytical method. The predictions are compared to actual thermocouple data from welds conducted under identical conditions, and are shown to he in good agreement. Although the method proposed in this work does not replace more accurate numerical analyses, it does provide guidance in weld parameter development. This is demonstrated through the model-based scaling of weld parameters for dissimilar tube welds over a range of tube diameters.

Introduction

Previous Thermal Models of Friction and Inertia Welding

In industrial friction and inertia welding production situations, it is not always possible to conduct extensive instrumented testing during which temperature data are gathered. Peak joint temperature and the temperature profile in the region near the weld can have a significant impact on flash formation, heat-affected zones, and joint strength. Cooling rates are closely related to joint temperature profiles and they directly influence the residual stress state developed in the joint. The issue of residual stress becomes more significant in dissimilar material joints. It is therefore desirable to have a means of rapidly and accurately estimating peak joint temperatures and cooling rates based on input parameters and routinely gathered inertia welding machine performance data.

The present model offers such estimates based on an analytical solution and two proposed parametric representations of the heat generation term. The model presented here is specifically for tubular cross sections, and the analytical models assume constant, but temperature-averaged, material properties. The only required inputs are the measured decay of the rotational speed, the moment of inertia of the flywheel, the total burnoff or reduction in length due to flash, and an assessment (or assumption) of how the burnoff is divided between the two tubes.

It is not the intent of this work to supplant more detailed numerical analyses of the inertia welding process, which are important in determining such mechanical aspects of the process as residual stress and flash formation. The present model is, however, sufficiently accurate to be used as a reduced-order thermal model for process optimization and parameter development in the inertia welding of tubes. A more accurate "truth" model, such as a finite element model, can then be used to further examine a more limited set of interesting parameters and quantify flash evolution and residual stress formation.

The first published analytical solution to the transient thermal history during friction welding is generally attributed to Rykalin, *et al.* (Ref. 1), although several of the same era researchers from the former Soviet Union also discussed heat input during friction welding (Refs. 2–4). The mathematics upon which this analytical solution is based appears, among other places, in the work of Carlslaw and Jaeger (Ref. 5). The model assumptions are semi-infinite solid; constant flux at the free surface for time t_h, then flux is "turned off"; zero initial temperature; and constant material properties. The solution is given by the following equation (Refs. 1, 5):

for $0 \le t \le t_h$:

$$T = \left(\frac{2q_o}{k}\right)\cdot\left\{\begin{array}{l}\sqrt{\frac{at}{p}}\exp\left(\frac{-x^2}{4at}\right)\\ -\frac{x}{2}\,erfc\left(\frac{x}{2\sqrt{at}}\right)\end{array}\right\}$$

$$= \left(\frac{2q_o}{k}\right)\cdot\sqrt{\alpha t}\cdot ierfc\left(\frac{x}{2\sqrt{\alpha t}}\right)$$

for $x > t_h$:

$$T = \left(\frac{2q_o}{k}\right)\left\{\begin{array}{l}\sqrt{\alpha t}\cdot ierfc\left(\frac{x}{2\sqrt{\alpha t}}\right)\\ -\sqrt{\alpha\left(t-t_h\right)}\\ \cdot\ ierfc\left(\frac{x}{2\sqrt{\alpha\left(t-t_h\right)}}\right)\end{array}\right\} \quad (1)$$

where k is the thermal conductivity, α is the thermal diffusivity, x is the distance

KEY WORDS

Inertia Welding
Friction Welding
Thermal Models
Dissimilar Tubes
Reduced Order Model
Weld Parameters

V. R. DAVÉ and M. J. COLA are with the Materials Science and Technology Div., Los Alamos National Laboratory, Los Alamos, N.Mex. G. N. A. HUSSEN is with the Materials Science and Engineering Dept., Stanford University, Palo Alto, Calif.

from the weld interface, and q_o is the magnitude of the surface heat flux.

The next significant contribution was made by Cheng (Refs. 6, 7), who analyzed both similar and dissimilar tubular joint configurations. Cheng numerically solved the differential equation of heat conduction (see Equation 2, which follows) with appropriate boundary conditions, and also allowed the material properties to vary with temperature (Ref. 6):

$$\frac{\partial T}{\partial t} + U(t)\frac{\partial T}{\partial x} = \frac{1}{\rho C_p}\frac{\partial}{\partial x}\left(k\frac{\partial T}{\partial x}\right) - \frac{\sigma \varepsilon P}{\rho C_p A}\left(T^4 - T_o^4\right) - \frac{hP}{\rho C_p A}\left(T - T_o\right) \quad (2)$$

where A is the cross-sectional area, T_o is the ambient temperature surrounding the tube, P is the outer perimeter of the tube, C_p is the specific heat, ρ is the density, h is the film coefficient of heat transfer (convective cooling), U(t) is the velocity of the melt front, ε is the emissivity, and σ is the Stefan-Boltzmann constant. Cheng allowed for the existence of a melt layer by incorporating a moving boundary term. Several experimental studies have refuted the notion of melting during friction welding, such as the work of Weiss and Hazlett (Ref. 8), and this topic will be revisited later in the present work. As Wang (Ref. 9) pointed out, it is quite likely that softened material at temperatures near the melting point will be expelled as flash before melting can occur.

Wang and Nagappan (Ref. 10) performed a thermal analysis similar to that of Cheng but for the inertia welding of steel bars. Their predictions showed the peak temperature to be less than the melting point and that for inertia welding, the peak temperatures are achieved very quickly as compared to conventional friction welding. Additionally, they noted a strong dependence of the predicted temperature distribution on the total welding time. This total welding time is a function of all the main process variables: initial rotational speed, thrust pressure, moment of inertia, etc. Their model has good qualitative agreement with measured temperature values.

Johnson, *et al.* (Ref. 11), have also noted the power dissipation curve for inertia welding is very different than that for friction welding. They have suggested a two-part curve: Stage I, corresponding to a more concentrated initial contact and Stage II, a slower (relatively slower) decay. They proposed the following functional forms:

$$\text{Stage } I: q(t) = q_{\max}\sin(\omega t)$$
$$\text{Stage } II: q(t) = T_{\max}\sqrt{\frac{k\rho C_p}{\pi t}} \quad (3)$$

where q_{max} is the maximum power dissipation and T_{max} is the maximum interface temperature attained — Fig. 1. A more recent moltistage thermal model for direct-drive friction welding was developed by Midling and Grong (Ref. 12), who proposed various analytical forms for the heating stage, steady-state condition, and cooling stage based on continuous planar disc sources at the weld interface.

There are numerous finite element and finite difference models on both conventional friction and inertia welding. These modeling efforts account for the heat generation term by examining the coupled thermomechanical problem together with an interfacial friction law. This interfacial friction law or constitutive relation must account for frictional heating. Sluzalec (Refs. 13, 14) was one of the first to use the finite element analysis (FEA) approach for friction welding, and Moal, *et al.* (Refs. 15, 16), have developed an FEA model specifically for inertia welding. Sahin, *et al.* (Refs. 17, 18), have produced a series of finite difference models. Weiss (Ref. 19) has also investigated the residual stresses after welding using the FEA approach. Fu and Duan (Ref. 20) have more recently used the FEA approach to model the axial pressure distribution in addition to the temperature field.

As mentioned earlier, this work is a reduced order model of the inertia welding process. It is motivated by the need to have simple, yet realistic, models that can be used for *in-situ* process monitoring and control and for rapid parameter development and validation. It differs from previous works in that it attempts to more accurately capture heat generation during welding as a function of time by using data routinely gathered by the inertia welding machine. This data is directly used as an input to the thermal simulation, which in this case is a reduced-order analytical model of heat conduction. As such, this approach could also be used with more sophisticated models for heat transfer, and would provide a reasonable estimate of heat generation without having to explicitly model the combined thermomechanical problem. Also, this approach is amenable to an on-line monitoring strategy that flags potentially defective welds in critical components and has the potential to alleviate the inspection burden by reducing it to "inspection for cause" as opposed to inspecting every component.

Equipment and Experimental Procedure

The commercially pure niobium and 316L stainless steel utilized in this study were in the form of 1 in.-diameter tubes. The Nb tube wall thickness was slightly thicker (0.125-in.) than the 316L tube wall (0.08 in.) to provide for greater forging action during the upset stage. Prior to

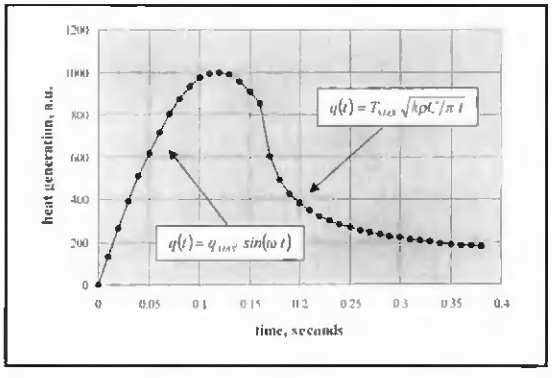

Fig. 1 — Schematic heat generation term after Johnson, et al. (Ref. 11).

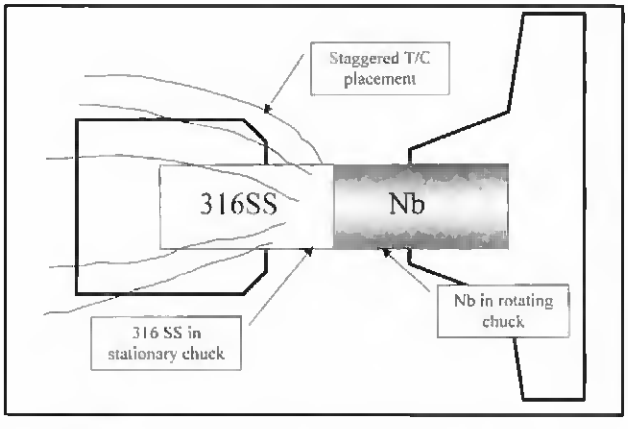

Fig. 2 — Schematic showing thermocouple placement.

Fig. 3 — Macrosection of the as-welded niobium-to-stainless steel joint.

inertia welding, the tubes were sectioned into 3-in. lengths and the faying surfaces were machined while flood cooled in isopropyl alcohol.

Inertia welds were produced using an MTI Model 90B inertia welding system. Initial emphasis was placed on determining parameters capable of producing joints that could sustain bending through 90 deg. Once suitable starting parameters were developed, welds were made at a surface velocity of 393 ft/min and axial force of 8330 lbf while maintaining a constant moment of inertia of 5.19 lbm-ft^2. After welding, and prior to testing, each joint was He leak checked, achieving a minimum leak rate of 1×10^{-10} atm.-cc/s.

Thermal cycle data were recorded by attaching 0.010-in.-diameter Type K (Chromel-Alumel) thermocouples to the outside of the stainless steel tube. Seven thermocouples were attached in 0.020-in. increments starting at the joint end of the tube and extending along its axis to 0.120 in. — Fig. 2. The data acquisition system was a National Instruments Board Model AT-MIO-16-10 connected to a Pentium-class computer running Labview SCXI 1120 software set at a gain of 20. A 10-kHz filter was used to record seven channels of thermocouple data at 200 Hz and store it for off-line analysis. Based on a thermocouple rise time analysis conducted by Sawada and Nishiwaki (Ref. 21), it is expected the thermocouple rise time could range from 10 to 50 ms, but is certainly expected to be less than 100 ms. The total bond time was less than 0.25 s for the welds made in this study, so the thermocouple may underestimate the peak temperature by, at most, 6% (assuming 50-ms rise time and peak temperature of ~1000°C occurring 0.1 s after the start of the bond). Data was sampled from the start of the weld cycle until the weld had cooled below 260°C. A macrosection of a completed weld between niobium and stainless is shown in Fig. 3.

The Heat Generation Term Derived Directly from Machine Measurements

Rykalin, *et al.* (Ref. 1), have determined the heat input during friction welding is given by the following:

$$q(t) = \text{const.} \cdot \mu \cdot p \cdot r \cdot \omega(t) \qquad (4)$$

Wang and Nagappan (Ref. 10) assumed the product of the friction coefficient μ and the normal pressure p remains a constant. By using this assumption — an empirical fit to the angular speed curve and a heat balance — they were able to derive an expression for the heat generation of the following form:

$$q(t) = \text{const.} \cdot r \cdot \omega(t) \qquad (5)$$

The present work takes two approaches to modeling heat input: a modification of Wang and Nagappan's treatment, and a second approach based purely on energy considerations. The first approach starts with Equation 5 and ignores radial variations on account of the thin-walled nature of the tubular sections being joined. Furthermore, heat generation at the interface is apportioned to each material according to the expression that applies to heat generation in an infinite composite solid (Ref. 5):

$$Q_1 + Q_2 = Q_{total}$$

$$\frac{Q_1}{Q_2} = \frac{k_1}{k_2} \cdot \sqrt{\frac{\alpha_2}{\alpha_1}} = \sqrt{\frac{k_1 \cdot \rho_1 \cdot C_1}{k_2 \cdot \rho_2 \cdot C_2}} \qquad (6)$$

The speed curve was modeled by the following empirical relationship:

$$\omega(t) = \omega_o \cdot \exp\left[-m \cdot \left(\frac{t}{\tau}\right)^n\right] \qquad (7)$$

where m and n are constants, and the characteristic time τ is defined as the time required for the rotational speed to decay to 10% of its original value at the start of the weld. The data in Fig. 4 shows the actual speed curve from a weld and the empirical form chosen to represent it. For the case shown here, normalized speed $[\omega(t)/\omega_o]$ is shown vs. time. The weld conditions were ω_o = 1488 rpm; I_o = 5.19 lbm-ft^2; P = 8330 lbf. The nonlinear, least-squares-fit parameters are m = 2.931 and n = 1.718. The heat input is then assumed to have the following form:

$$Q(t) = A_o \cdot \omega(t) \qquad (8)$$

where Q is the total heat input in watts, ω is the speed curve as represented by Equation 7, and A_o is a constant. The constant is evaluated based on conservation of energy. Before this can be done, it is recognized that some of the energy available to the joint from the flywheel will be used to heat and expel flash. Therefore,

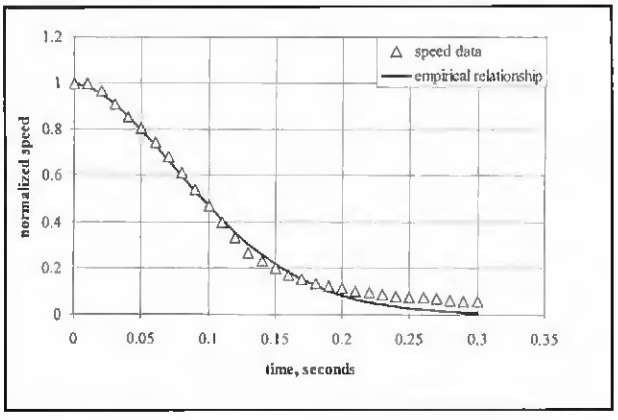

Fig. 4 — The angular speed curve as modeled empirically by Equation 7.

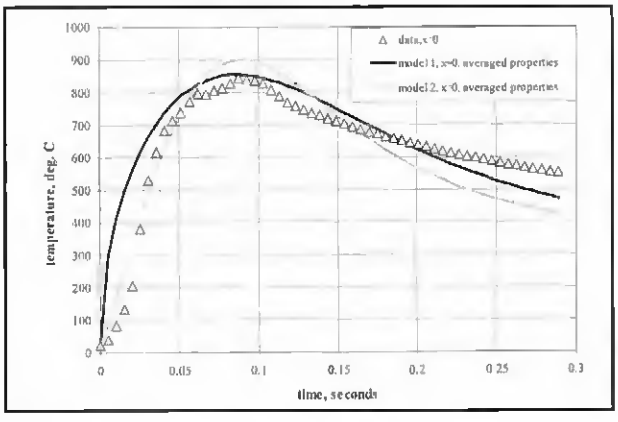

Fig. 5 — Comparison between predicted and actual thermal profiles on the stainless side of the weld.

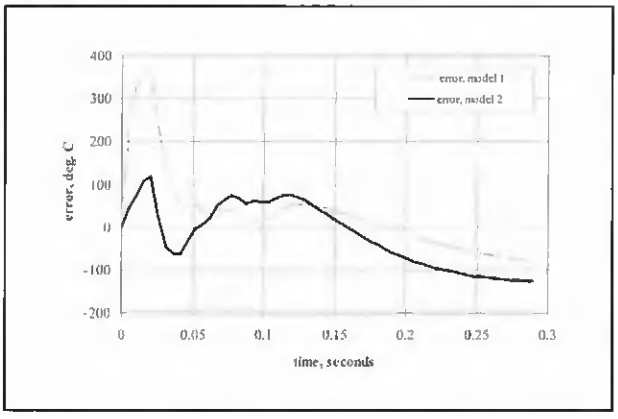

Fig. 6 — Error as defined by Equation 14 shown as a function of time for Models 1 and 2.

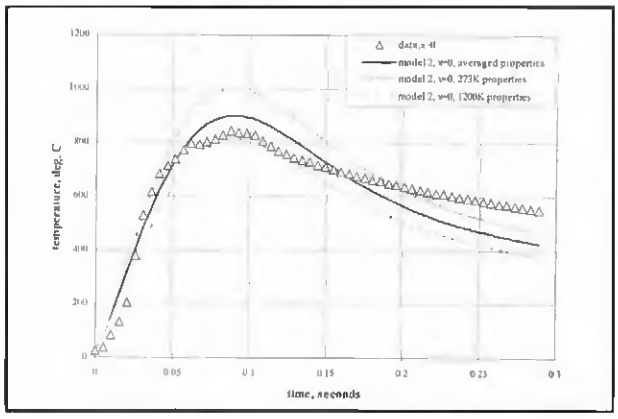

Fig. 7 — The effect of variations in thermomechanical properties on model predictions.

the effective energy conducted into the workpiece will be less than the initial energy of the flywheel. The approach taken in this work was to examine the joint after the weld and make a determination as to the amount of material expelled from each side. For example, in the case of dissimilar welds between Nb and 316L stainless, the flash was expelled almost entirely in the Nb. The inertia welding machine tracks the reduction in length during the weld, and, therefore, it is possible to know the burnoff directly from machine measurements. Then it is assumed the flash carries off an amount of energy equal to

$$E_{flash} = B \cdot A_C \cdot \rho \cdot \bar{C} \cdot \Delta T_{MAX} \qquad (9)$$

where B is the total reduction in length, or burnoff; A_C is the cross-sectional area of the tube; ρ is the density; $\bar{C}$ is the average specific heat over the temperature range ΔT_{MAX}; and ΔT_{MAX} is the maximum temperature rise.

Since the maximum temperature attained is not known *a priori*, an iterative procedure must be used. The peak joint temperature is first estimated, the energy lost to flash is then evaluated, the resulting thermal profile is calculated, and the process is repeated until the maximum predicted temperature matches the estimate. The constant A_0 can now be evaluated:

$$Q(t) = A_O \cdot \omega(t)$$

$$\int_0^\infty Q(t')dt' = (E_O - E_{flash})$$

so

$$A_O = \frac{(E_O - E_{flash})}{\int_0^\infty \omega(t')dt'}$$

$$\text{where } E_O = \frac{1}{2} I_O \omega_O^2 \qquad (10)$$

The second method of determining the heat flux involves direct consideration of the dissipation of rotational kinetic energy by the weld. For any given time during the weld, it can be generally said the following expression relates the energy dissipated by the weld to the loss in kinetic energy of the flywheel:

$$E_{weld}(t) = \frac{1}{2} I_O \omega_O^2 - \frac{1}{2} I_O [\omega(t)]^2 \qquad (11)$$

Therefore, it is immediately observed that the power dissipation in the weld is given by the following:

$$Q(t) = -I_O \omega(t) \cdot \frac{d\omega}{dt} \qquad (12)$$

This ignores stored elastic energy in the tooling or inertia welding machine and also ignores other energy losses such as machine friction and grip "slippage," *i.e.*, energy loss at the workpiece/tool interface. It turns out this method was independently discovered by Dr. H. A. Nied, Sr., of General Electric Co., and was brought to the authors' attention through Ref. 22. Using the same model for the rotational speed as shown in Equation 7, the total power dissipation in the weld is assumed to be the following:

$$Q(t) = C_O \cdot \frac{m \cdot n}{\tau} \cdot \exp\left[-2 \cdot m \cdot \left(\frac{t}{\tau}\right)^n\right] \cdot \left(\frac{t}{\tau}\right)^{n-1} \qquad (13)$$

As before, the constant C_0 takes into account the fact that some of the energy dissipated in the weld must go into heating and expelling the flash. C_0 is calculated in an entirely analogous manner to A_0 and is given by the following:

$$C_O = 1 - \frac{E_{flash}}{E_O} \qquad (14)$$

The thermal profiles can now be evaluated with the aid of Duhamel's theorem, as applied to the case of 1-D heat conduction in a semi-infinite solid with a time-varying flux at the free surface, as follows:

$$T(x,t) = \frac{1}{k}\sqrt{\frac{\alpha}{\pi}} \cdot \int_0^t q(t-\zeta) \cdot \exp\left(\frac{-x^2}{4\alpha\zeta}\right) \cdot \frac{d\zeta}{\sqrt{\zeta}} \qquad (15)$$

where q(t) is the time-varying surface flux.

The heat flux q is easily derived from the expressions for total power shown in Equations 8 and 13 by considering the cross-sectional area and the fraction of energy entering into a particular side of the joint, as follows:

$$q_1(t) = \frac{Q_{total}(t)}{A_C} \cdot \frac{1}{1 + \sqrt{\frac{k_2 \cdot \rho_2 \cdot C_2}{k_1 \cdot \rho_1 \cdot C_1}}} \qquad (16)$$

For the two proposed heat inputs, the thermal profiles will now be compared for a stainless steel-to-niobium weld. The weld parameter data and assumed thermal properties of the materials are shown in Table 1. The resulting thermal profiles are shown in Figure 5 and are compared to the actual data at the position of the weld interface, *i.e.*, x = 0. Model 1 refers to the heat flux as specified by Equation 8, whereas Model 2 refers to the heat flux as given by Equation 13.

A measure of how well the two models represent the data can be deduced by considering the error as a function of time:

$$\text{Error}(t) \equiv M(t) - Y(t) \qquad (17)$$

where M(t) is the predicted temperature at t and Y(t) is the measured temperature at t.

Table 1 — Weld Parameter Data and Assumed Thermal Properties

Quantity (all thermophysical data from Ref. 20)	Value
Initial Rotational Speed	1487 rpm (1500 nominal)
Moment of Inertia	5.19 lb-ft^2
Axial Welding Force	8330 lb
Average Specific Heat for Nb over 273–1273 K	0.29 J/g/K
Average Thermal Conductivity for Nb over 273–1273 K	0.59 W/cm/K
Average Specific Heat for 316 SS over 273–1273 K	0.56 J/g/K
Average Thermal Conductivity for 316 SS over temperature range 273–1200 K	0.21 W/cm/K
Fraction of total power going to 316 SS side (equation 16)	0.445
Fraction of total power going to Nb side	0.555

Table 2 — Comparison Between Subscale and Fullscale Inertia Weld Parameters

Parameter	Value
Full-scale Inertia	5.19 lb-ft^2
Subscale Inertia	3.32 lb-ft^2
Full-scale Initial Speed	1570 rpm
Subscale Initial Speed	1675 rpm
Full-scale Area	0.231 in.^{2}
Subscale Area	0.168 in.^{2}
Bond Pressure (held constant as area changes)	25854 lb/in.^{2}

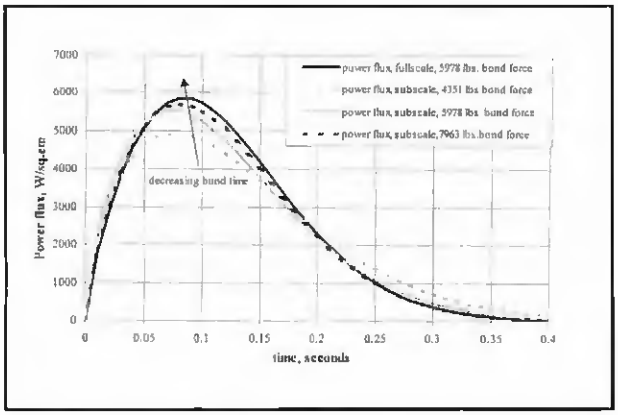

Fig. 8 — A comparison between the power dissipation during the bond for the full-scale bond and the subscale bond conducted at various bond forces.

The evolution of the error is shown in Fig. 6 for the two models under consideration. It is clear Model 2 better represents the data at short times, whereas Model 1 seems to be more suitable at long times. Another important factor that has been ignored in the treatment thus far is the effect of temperature-dependent material properties. This effect is shown in Fig. 7 by changing the assumed material properties for conduction through the stainless steel.

Heat Input Model as a Basis for Selection of Weld Parameters

It will now be shown that the proposed heat generation term can be used to select weld parameters as part size is changed, *i.e.*, the parameter-scaling problem. The basic assumption in inertia welding is that the energy per unit area of the joint must be kept constant as the weld parameters are scaled for larger or smaller diameters. This means the following, with E specified by the initial flywheel kinetic energy:

$$\frac{E_1}{A_1} = \frac{E_2}{A_2} \qquad (18)$$

The nominal bond pressure is usually not altered as the size is increased, although the bond force is adjusted to make the bond pressure constant. In the present treatment, the effect of pressure is considered and modifications to the bond pressure with size are proposed. The effect of increasing pressure is tracked by a close examination of the power dissipation curves, and joints made in components of different sizes are considered "equivalent" when their respective power dissipation curves resemble one another.

The behavior of the hot, highly worked interfacial layer that forms during the inertia weld can generally be modeled using the following phenomenological form (Ref. 15):

$$\tau = (\text{const.})\cdot(\Delta V)^p \cdot P^q \qquad (19)$$

where τ is the shear stress, ΔV is the relative slip velocity, and P is the interfacial bond pressure.

The slip velocity for thin-walled tubes is given by $v = \omega r$, where r is the average radius. The expression for the tangential shear (radial shear effects ignored) stress then becomes the following:

$$\tau(t) = (\text{const.})\left[\omega(t)\cdot r\right]^p \cdot P^q$$

or

$$\frac{\tau(t)}{\left[\omega(t)\right]^p} = (\text{const.})\cdot r^p \cdot P^q \qquad (20)$$

The quantities on the left-hand side of Equation 20 are directly related to the heat input and power dissipation during the weld. Therefore, if it is assumed the power dissipation is to be held constant as the part size changes, then this suggests an additional scaling law (in addition to Equation 18):

$$r^p \cdot P^q = (\text{const.}) \qquad (21)$$

In the present work, it was assumed that $p = q = 1$ in Equation 21 for purposes of testing the newly proposed scaling law. First, welds were produced between titanium and niobium using only Equation 18, *i.e.*, keeping the initial bond energy per unit area a constant. The interfacial bond pressure was also held constant. The subscale tube diameter was 0.75 in., and the full scale was 1 in. The bond parameters for both bonds based purely on Equation 18 and constant interfacial bond pressure are shown in Table 2.

The full-scale bonds made under these conditions easily passed a destructive bend test (samples were bent after flash was removed and a bend angle of greater than 45 deg was achieved before failure at the joint), whereas the subscale samples failed immediately upon being subjected to bending loads (essentially zero bend angle). Clearly the assumed scaling law based purely on Equation 18 and a constant interfacial bond pressure did not work. The bond pressure was then modified based on Equation 21 with exponents p and q equal to 1. The original bond pressure based on constant bond pressure was 5978 lbf. The bond pressure predicted by Equation 21 with $p = q = 1$ is 7963 lbf. The full-scale bond was conducted at a bond pressure of 5978 lbf. Based on the data in Fig. 8, as the subscale and full-scale power curves start to resemble one another, the resulting bonds are expected to have comparable bond quality. The sample bend tests also suggest this is the case. This means the power dissipation curve can provide valuable guidance in the selection of bond parameters as the size of the joint changes. The assumption of $p = q = 1$ is somewhat arbitrary, but importance should not be attached to the specific

values of these parameters. The central message of this study is that the power dissipation characteristic as a function of time is a good means of transferring weld parameters from one part size to a smaller or larger size.

Inertia Welding Heat Generation and the Possible Existence of a Liquid Interlayer

There has been and continues to be some debate about the possible existence of a liquid layer during inertia or friction welding. Cheng (Refs. 6, 7) allowed for the existence of such a molten layer in his modeling work. Several experimental studies by Squires (Ref. 23), Weiss, and Hazlett (Ref. 8), and Hasui, *et al.* (Ref. 24), did not find evidence of melting. Wang and Nagappan (Ref. 10) predicted the peak temperatures would be below the melting point based on their modeling work of inertia-welded steel bars. Wang (Ref. 9) points out available metallurgical investigation does not support the existence of a liquid film at the interface, and torque measurements do not show a disruption or sudden drop that may be expected on account of a liquid interlayer.

To further analyze the possibility of melting during the inertia bonds made in this work, the possibility of a fluid layer subjected to shear is considered. A predicted melt layer thickness will now be derived for such a layer by invoking simple hydrodynamic reasoning. The laminar boundary layer thickness is specified by the following:

$$\delta \approx \sqrt{\frac{\nu \cdot x}{U_\infty}} \qquad (22)$$

where x is the position along the wall in the direction of flow, v is the kinematic viscosity, and U_∞ is the free-stream velocity.

The average velocity during the speed curve decay is obtained by finding the average value of the speed curve shown in Equation 7 using fit parameters as described in Fig. 4. This results in an average velocity of 0.93 m/s. The dynamic viscosity of molten iron ranges from 5 to 10 centipoise (a centipoise, cP, is equal to 10^{-3} kg·m^{-1}·s^{-1}) over a range of temperatures (Ref. 25), and this equates to a kinematic viscosity of $6 \times 10^{-7} - 1.2 \times 10^{-6}$ m^2/s. The distance x is the maximum distance the part may rotate during the inertia weld, which in this case is the total circumferential travel during the decay in rotational velocity. Again using Equation 7 for the conditions described in Fig. 3, the part makes a total of 2.5 rotations, so the maximum possible travel distance is 0.2 m. Therefore, the Reynolds Number of this flow is the following:

$$\mathrm{Re} \equiv \frac{U_\infty x}{\nu} = \frac{(0.93\ \mathrm{m/s}) \cdot (0.2\ \mathrm{m})}{\left(1 \times 10^{-6}\ \mathrm{m^2/s}\right)}$$

$$= 1.86 \times 10^5 \qquad (23)$$

which is within the laminar regime. The corresponding film thickness then becomes

$$\delta = \sqrt{\frac{\nu \cdot x}{U_\infty}}$$

$$= \sqrt{\frac{\left(1 \times 10^{-6}\ \mathrm{m^2/s}\right) \cdot (0.2\ \mathrm{m})}{(0.93\ \mathrm{m/s})}}$$

$$= 464 \mu\mathrm{m} \qquad (24)$$

From microstructural investigation, there is no evidence of a 400+ micron-wide melt layer that, if it did exist, would be most conspicuous and easily detectable. Furthermore, even on submicron-length scales, no evidence of melting was detected. At the interface, there was an intermetallic reaction layer consisting of a Nb-Fe-Cr intermetallic compound that was approximately 200 nm thick. If we assume this layer was formed by liquid-phase reaction, we can approximate the thickness of the laminar boundary layer to be the width of this reaction zone. In that case, using Equation 22, the equivalent metal viscosity would have been approximately 2×10^{-10} cP, which is a physically unrealistic number for molten metals. It is, therefore, reasonable to assume there was no melting during the welding process.

Conclusions and Future Work

In this study of the heat generation term during inertia welding of dissimilar tubes, the following was demonstrated:

1) The temperature profile during inertia welding can be well represented by simple analytical solutions that directly use machine-generated data.

2) The proposed forms of the heat generation term can be used to provide guidance for parameter development when attempting to transfer successful weld parameters to varying part diameters.

3) It is unlikely a fluid layer was generated during the inertia welds discussed in this work.

The heat generation terms represented by Equations 8 and 13 could also be used as part of an *in-situ* process monitoring methodology. If the heat generation term, the effective bond time (time required for angular speed to drop to 10% of its initial value), the material burnoff, and the burnoff rate are all monitored, it may be possible to establish a process window based solely on *in-situ* measurements, which would be the first step toward a 100% quality-assured methodology for inertia welding (no postprocess inspection required). Accounting for temperature-dependent material properties can enhance the thermal predictions in this work, and such simulations are in progress.

Acknowledgments

This research was funded under DOE contract No. W-7405-ENG-36. The authors also wish to thank Ann M. Kelly for her valuable assistance in metallography, Dr. David F. Teter for his valuable suggestions and electron microscopy work, and Dr. R. D. Dixon for his critical review of the manuscript.

References

1. Rykalin, N. N., Pugin, A. I., and Vasil'eva, V. A. 1959. The heating and cooling of rods butt-welded by the friction process. *Svarochnoe Proizvodstvo (Welding Production)*: 42–52.

2. Vill', V. I. 1959. Energy distribution in the friction welding of steel bars. *Svarochnoe Proizvodstvo (Welding Production)*: 31–51.

3. Gel'dman, A. S., and Sander, M. P. 1959. Power and heating in the friction welding of thick-walled steel pipes. *Svarochnoe Proizvodstvo (Welding Production)*: 53–61.

4. Zadegson, R. I., and Voznessenskii, V. D. 1959. Power and heat parameters of friction welding. *Svarochnoe Proizvodstvo (Welding Production)*: 63–70.

5. Carlslaw, H. S., and Jaeger, J. C. 1959. *Conduction of Heat in Solids*. Oxford, U.K.: Clarendon Press.

6. Cheng, C. J. 1962. Transient temperature distribution during friction welding of two similar materials in tubular form. *Welding Journal* 41(12): 542-s to 550-s.

7. Cheng, C. J. 1963. Transient temperature distribution during friction welding of two dissimilar materials in tubular form. *Welding Journal* 42(5): 233-s to 240-s.

8. Weiss, H. D., and Hazlett, T. H. 1966. The role of material properties and interface temperatures in friction welding dissimilar metals. *ASME Paper 66-MET-8*.

9. Wang, K. K. 1975. Friction welding. *WRC Bulletin no. 204*.

10. Wang, K. K., and Nagappan, P. 1970. Transient temperature distribution in inertia welding of steels. *Welding Journal* 49(9): 419-s to 426-s.

11. Johnson, P. C., Stein, B. A., and Davis, R. S. 1966. Inertia Welding. Unpublished technical report, Caterpillar Tractor Co.

12. Midling, O. T., and Grong, O. 1994. A process model for friction welding of Al-Mg-Si alloys and Al-SiC metal matrix composites — I: HAZ temperature and strain rate distrib-

ution. *Acta Metallugica et Materialia* 42(5): 1595–1609.

13. Sluzalec, A. 1985. Thermoplastic effects in friction welding analyzed by finite element method. *The Effects of Fabrication Related Stresses on Product Manufacture and Performance, TWI Conference Proceedings*. The Welding Institute, Abington, U.K. Paper –8.

14. Sluzalec, A. 1990. Thermal effects in friction welding. *Int. J. of Mech. Sci.* 32(6): 467–478.

15. Moal, A., Massoni, E., and Chenot, J-L. 1990. A finite element modeling for the inertia welding process. *Conference on Computational Plasticity: Fundamentals and Applications I*, pp. 289–300. Swansea, U. K.: Pineridge Press.

16. Moal, A., and Massoni, E. 1995. Finite element modeling of the inertia welding of two similar parts. *Engineering Computations* 12(6): 497–512.

17. Sahin, A. Z., Yilbas, B. S., and Al-Garni, A. Z. 1996. Friction welding of Al-Al, Al-steel, and steel-steel samples. *J. of Mat Eng. and Per.* 5(1): 89–99.

18. Sahin, A. Z., Yilbas, B. S., Ahmed, M., and Nickel, J. 1998. Analysis of the friction welding process in relation to the welding of copper and steel bars. *J. of Mat. Proc. And Tech.* 82: 127–136.

19. Weiss, R. 1998. Residual stresses and strength of friction welded ceramic/metal joints. *Welding Journal* 77(3): 115-s to 122-s.

20. Fu, L., and Duan, L. 1998. The coupled deformation and heat flow analysis by finite element method during friction welding. *Welding Journal* 77(5): 202-s to 207-s.

21. Sawada, T., and Nishiwaki, N. 1991. Response of a thermocouple to transient temperature changes in a metal to which it is attached. *Int. J. Mech. Sci* 33(7): 551–561.

22. Communication with Tom McGaughy of the Edison Welding Institute (EWI), 10/20/99, who distributed a copy of EWI CRP Report SR9821, *Inertia Welding of IN718 and 1045 Steel: Numerical Modeling and Experiments*.

23. Squires, I. F. 1966. Thermal and mechanical characteristics of friction welding mild steel. *British Welding Journal* 13(11): 652–657.

24. Hasui, *et al.* 1968. Experimental studies on friction welding phenomena. *Trans. Nat. Res. Inst. Metals Japan* 10(4): 53–71.

25. Geiger, G. H., and Poirier, D. R. 1973. *Transport Phenomena in Metallurgy*. Reading, Mass.: Addison Wesley Publishing Co.

Preparation of Manuscripts for Submission to the *Welding Journal* Research Supplement

All authors should address themselves to the following questions when writing papers for submission to the Welding Research Supplement:

- Why was the work done?
- What was done?
- What was found?
- What is the significance of your results?
- What are your most important conclusions?

With those questions in mind, most authors can logically organize their material along the following lines, using suitable headings and subheadings to divide the paper.

1) **Abstract.** A concise summary of the major elements of the presentation, not exceeding 200 words, to help the reader decide if the information is for him or her.

2) **Introduction.** A short statement giving relevant background, purpose and scope to help orient the reader. Do not duplicate the abstract.

3) **Experimental Procedure, Materials, Equipment.**

4) **Results, Discussion.** The facts or data obtained and their evaluation.

5) **Conclusion.** An evaluation and interpretation of your results. Most often, this is what the readers remember.

6) **Acknowledgment, References, and Appendix.**

Keep in mind that proper use of terms, abbreviations and symbols are important considerations in processing a manuscript for publication. For welding terminology, the *Welding Journal* adheres to ANSI/AWS A3.0-94, *Standard Welding Terms and Definitions*.

Papers submitted for consideration in the Welding Research Supplement are required to undergo Peer Review before acceptance for publication. Submit an original and one copy (double-spaced, with 1-in. margins on 8 ½ x 11-in. or A4 paper) of the manuscript. Submit the abstract only on a computer disk. The preferred format is from any Macintosh® word processor on a 3.5-in. double- or high-density disk. Other acceptable formats include ASCII text, Windows™ or DOS. A manuscript submission form should accompany the manuscript.

Tables and figures should be separate from the manuscript copy and only high-quality figures will be published. Figures should be original line art or glossy photos. Special instructions are required if figures are submitted by electronic means. To receive complete instructions and the manuscript submission form, please contact the Peer Review Coordinator, Doreen Kubish, at (305) 443-9353, ext. 275; FAX 305-443-7404; or write to the American Welding Society, 550 NW LeJeune Rd., Miami, FL 33126.